High-Frequency Directivity in Strong Ground Motion Modeling Methods

Frantisek Gallovic[1*] and Jan Burjanek[1]

[1] *Department of Geophysics, Faculty of Mathematics and Physics, Charles University, V Holesovickach 2, Prague 8, 180 00, Czech Republic;*

[*] *Author for correspondence:*

Frantisek Gallovic

Department of Geophysics

Faculty of Mathematics and Physics

Charles University

V Holesovickach 2

Prague 8, 180 00

Czech Republic

e-mail: gallovic@karel.troja.mff.cuni.cz

tel.: +420221912535

fax.: +420221912555

Submitted to Annals of Geophysics (revised version).

Abstract

We are investigating two distinct strong ground motion simulation techniques as regards their high-frequency directivity: i) the composite model with a fractal subevent size distribution, based on the method of summation of empirical Green's functions, and ii) the integral model with the k-squared slip model with k-dependent rise time, based on the representation theorem. We test the simulations in a 1D layered crustal model against empirical PGA attenuation relations, particularly with regard to their uncertainty, described by the standard deviation (σ). We assume that any synthetic model for a particular earthquake should not provide a PGA scatter larger than the observed scatter for a large set of earthquakes. The 1999 Athens earthquake (M_w=5.9) is studied as a test example. In the composite method, the synthetic data display a scatter of less than $\pm 2\sigma$ around the empirical mean. The k-squared method displays a larger scatter, demonstrating strong high-frequency directivity. It is shown that the latter can be reduced by introducing a formal spectral modification.

1 Introduction

Low-frequency directivity effects are well known. For example, there is a number of seismic recordings of recent earthquakes (e.g., 1992 Landers, 1994 Northridge, 1995 Kobe, 1999 Chi-Chi), which show long-period velocity pulses caused by rupture propagation towards a station. This effect can be successfully explained by the apparent source time function varying with azimuth (Haskell, 1964).

However, high-frequency directivity is different. Somerville et al. (1997) showed on empirical data that the effect of directivity vanishes for short-period ground motions. Boatwright and Boore (1982) suggested that the total variation of PGA should not exceed a factor of 10.

Hartzell et al. (1999) compared several strong ground motion modeling techniques applied to the 1994 Northridge earthquake. However, they did not discuss the directivity effect inherent to the compared source models although it can drastically change the overall synthetic results (e.g., PGA maps). In their study, the techniques under comparison were based on two kinds of earthquake source descriptions - composite and integral models. The composite model is understood to be a discrete sequence of independently rupturing subevents. The integral model utilizes the representation theorem with prescribed spatial-temporal distribution of the dislocation over the fault. In this paper we adopt two representative approaches of the composite and integral methods with the same fundamental features as those in the paper by Hartzell et al. (1999), see further.

We compare the high-frequency directivity of these two source models in a given crustal model. The main assumption is that any synthetic (source + crustal) model for one particular earthquake should not provide an uncertainty of strong-motion characteristics larger than the uncertainty observed for a general set of earthquakes. Note that this assumption has to be understood as an empirical constraint on the physical parameters of the simulation model and/or on the simulation method itself.

In particular, we choose PGA as the studied characteristic since it is sensitive to high-frequency directivity. We expect at least 95% of the simulated PGAs to fall within the

$\pm 2\sigma$ range around the mean empirical attenuation curve. Such comparison could disprove the modeling techniques that break systematically (not only for one worst case scenario) the $\pm 2\sigma$ bounds if the attenuation relations are obtained from a sufficiently large data set. However, it cannot be used for technique validation unless we take into account all possible phenomena that boost the scatter of the simulation (e.g., 3D structural effects, site effects, etc.). Note that PGA is just one special choice and that a similar comparison can be carried out for any other characteristics, e.g. duration, spectral levels at given frequencies, Arias intensity, etc.

2 Simulation techniques

Composite models are based on the assumption that the modeled event can be seen as a discrete sequence of independently rupturing subevents. We implement the composite model with fractal subevent size distribution (hereinafter only FSSD) described by Hartzell et al. (1999). The number of subevents with a characteristic dimension greater than R is proportional to R^{-2}. The subevents do not overlap, and the sum of their areas equals the area of the target event. The subevents are distributed randomly over the fault, creating a typical fractal pattern. Both the final slip and duration of each subevent are related to its characteristic dimension, using constant stress-drop scaling. The subevents' source time functions are modeled using a simple point-source approximation (Brune, 1970) with corner frequency

$$f_c = cv_r/R, \tag{1}$$

where v_r is the rupture velocity. The constant of proportionality c characterizes the efficiency of the subevent high-frequency radiation given by subevent heterogeneity (e.g., in its spatial stress drop distribution). We consider it to be a free parameter of the model. A detailed description can be found in Burjanek (2002).

In the integral models one prescribes the spatial-temporal evolution of the slip over the fault. Bernard and Herrero (1994) proposed a stochastic model with a k^{-2} slip distribution, k being the wave number. This means that the decay of the slip wave number amplitude spectrum is proportional to k^{-2} for large wave numbers, and its phase is random. This model, however, does not include asperities, which are a common feature of slip inversion results (Somerville et al., 1999). To include asperities in the slip model, we adopt the so-called hybrid slip, which is a combination of the long-wavelength deterministic part (asperities) and short-wavelength stochastic part (random phase in spatial slip spectrum), preserving the k^{-2} spectral decay of the slip amplitude spectrum (see Gallovic and Brokesova, 2004a). In this model, hereinafter referred to as the k-squared model, the rupture propagates with constant velocity v_r in the form of a slip pulse of width L_0. Small-scale slip inhomogeneities rupture within a time proportional to their spatial wavelength (Bernard et al., 1996). This results in a non-uniform shape of the slip rate functions over the fault.

Note that both models, the FSSD and k-squared, display an omega-squared falloff in displacement source spectra, i.e. a high-frequency plateau in the acceleration source spectra.

3 Benchmark – 1999 Athens earthquake

We use two source models to simulate strong ground motions due to the 1999 Athens earthquake (Tselentis and Zahradnik, 2000). We consider 112 virtual receivers distributed radially around the epicenter along 16 profiles at epicentral distances of 4 to 28 km (shown later in Fig. 3A). This station geometry has been chosen in order to compare the simulation results with the latest PGA attenuation relations for Greece by Skarlatoudis et al. (2003) defined with respect to the epicentral distance. The relations were obtained from a data set of 225 earthquakes, mainly normal and strike-slip events with magnitudes of $4.5 \leq M \leq 7.0$. More specifically, we choose their attenuation curve for rock sites (class B, NEHRP, 1994), normal faulting and magnitude of the Athens earthquake ($M_w = 5.9$). All calculations are carried out up to 10 Hz as spectral amplitudes at higher frequencies were found to diminish due to near-surface attenuation (see also Margaris and Boore, 1998).

Note that the Athens earthquake is a representative of predominantly unilateral earthquakes, in which case we expect a significant directivity effect. The unilaterality of the rupture propagation does not seem to be not an extreme scenario since, e.g., McGuire et al. (2002) showed that unilateral earthquakes predominate in the global earthquake catalog.

3.1 Source and propagation models

We adopt the seismic moment 7.8×10^{17}Nm, epicentral location (38.08^{o}N, 23.58^{o}E), depth 12km, focal mechanism (strike 123^o, dip 55^o, rake -84^o) and the fault orientation from previous studies (for review see Zahradnik, 2002). The remaining parameters, i.e. length

11km and width 8km of the fault and asperity slip contrast 2 (necessary for the k-squared model with asperity only), are taken from the empirical relations of Somerville et al. (1999). The asperity slip contrast is defined as the ratio between the mean slip on asperity and mean slip on the whole fault. Somerville et al. (1999) also suggested one or two asperities covering 1/4 of the whole fault. For simplicity, we consider just one asperity. According to Plicka and Zahradnik (2002) we assume that the nucleation point (corresponding to the hypocenter) is located in the bottom-left corner of the asperity. The rupture is assumed to propagate radially at a constant rupture velocity $v_r = 2.8$km/s.

The remaining free parameters (c for FSSD and L_0 for the k-squared models) are difficult to determine from empirical relations. We thus set them by trial-and-error ($c = 0.9$, $L_0 = 2.4$km) to get the highest synthetic PGAs just below the $mean{+}2\sigma$ bound of empirical PGA attenuation. We have found that parameter c in the FSSD model affects only the absolute level of the PGA values, not their scatter. Concerning the k-squared model, Brune's pulse is used as the slip velocity function. Parameter L_0 affects only the PGAs at the receivers in the direction of rupture propagation, leading to slight changes (up to 10%) in the PGA scatter. The k-squared model with the same parameters has also been tested by Gallovic and Brokesova (2004b) against macroseismic data. Fig. 1 shows an example of the slip distribution used in the k-squared method.

Green's functions (GF) are computed for a 1D isotropic crustal model with homogeneous layers (Tselentis and Zahradnik, 2000). In case of the FSSD model, we apply the discrete wave number method (Bouchon, 1981) to get full wavefield GFs for all subevent-station pairs. However, in the k-squared model, dense discretization of the fault is required,

so that a large number of GFs is needed. Since we are interested in PGAs at relatively short epicentral distances, we use the ray theory and consider the direct S-wave only. Fig. 2 shows a comparison of the full wavefield and direct S-wave accelerograms (using the k-squared model) for one selected station marked in Fig. 3A. The station was chosen because of its position with respect to the fault where we expect the largest difference: It lies in the backward directivity zone, in the direction of the S-wave minimum and at the largest considered epicentral distance, where interference and/or reflected/refracted waves could be significant. Although the peaks do not coincide, the PGA values are in good agreement. An even better agreement was obtained for a few other neighboring stations of the same epicentral distance (not presented here), so that we believe that such an approximation of GF is acceptable for the given crustal model.

3.2 Results

We have computed the acceleration time histories at the 112 receivers using both methods. The computation is repeated for 10 realizations of the source random component (spatial distribution of subevents in the FSSD and slip phase in k-squared).

Mean PGA maps are shown in Fig. 3A. Both maps exhibit strong azimuthal variations. The maxima are located at about the same positions and reach similar values of about 4 m/s^2. The FSSD model provides two lobes of high PGAs next to the epicenter, in which one recognizes the combined effect of the directivity and S-wave radiation pattern. At larger epicentral distances, the PGA decays more or less regularly in all directions. On the

contrary, the map provided by the k-squared model is dominated by a single high-PGA spot. From this spot, the PGA values decay much more steeply to the west than to the south-east (i.e. the direction of rupture propagation). This particular shape is caused mostly by the directivity effect.

Fig. 3B shows all the simulated PGAs plotted with respect to the epicentral distance. The mean PGAs for given epicentral bins (gray strokes) roughly follow the overall decreasing trend of the mean attenuation curve. The mean PGAs at 4 and 8 km deviate from the trend. We ascribe this to the problem of epicentral distance that was adopted in the empirical attenuation relations. It is well known that this problem can be solved by different parametrization of the distance (distance from the fault, its surface projection, etc.). The trend of the mean PGAs also slightly differs from the empirical mean curve. This can be explained by the fact that depth and focal mechanism dependencies were not considered in the attenuation relations. Another problem could be an inappropriate crustal model adopted in the present study. The improvement of the fit with the empirical mean curve is beyond the scope of our paper.

We can see that in the FSSD method all the synthetic PGAs fall within the $\pm 2\sigma$ bounds around the empirical mean. The k-squared method yields a larger PGA scatter: all the PGAs fall under the $+2\sigma$ bound, however the lower bound -2σ is exceeded. We find that these low values come from stations located backwards to the direction of rupture propagation and are observed for each of all the stochastic realizations. Thus, the large scatter is caused by strong directivity in the k-squared method.

We explain the different PGA scatters of the two techniques by the different method-

ology used in high-frequency wave field modeling. In the FSSD model, the superposition of the subevents' time histories becomes incoherent for frequencies higher than the corner frequency of the smallest subevent. Thereby, constructive interference disappears and the resulting amplitude spectrum (plateau) is the RMS of the point-source subevent spectral plateaus (e.g., Frankel, 1991), independently of the direction of rupture propagation. On the contrary, in the k-squared method, the resulting high-frequency plateau comes from coherent summation, i.e. constructive interference. The height of the plateau depends on the direction of the rupture propagation at all frequencies (see Fig. 4a), which clearly explains the strong directivity of the k-squared model.

3.3 Modification of the k-squared method

Following Bernard and Herrero (1994), we can reduce the strong directivity by introducing a formal spectral modification. Its aim is to mimic the independence of the spectral plateau on the direction of rupture propagation as in the composite methods.

Gallovic and Brokesova (2004a) have shown, for line fault and Fraunhofer approximations, that the height of the high-frequency spectral plateau for the k-squared model is

$$A(\theta) \propto C_d(\theta)^2 X(aC_d(\theta)), \tag{2}$$

where C_d is the coefficient of directivity (Joyner, 1991) depending on the angle θ between the station and the direction of rupture propagation, X corresponds to the Fourier spectrum of the slip velocity function, and a is a parameter affecting the wave-number

dependence of the rise time (introduced by Bernard et al., 1996).

Bernard and Herrero (1994) proposed an even more heterogeneous rupture process at small scales, particularly, at scales smaller than the slip pulse width. This leads to more complicated slip velocity functions, stochastic at high frequencies. Those authors presume that the constructive interference disappears for frequencies higher than about $f_0 = v_r/L_0$ and the resulting height of amplitude spectral plateau becomes the same for all directions,

$$A_0 \propto RMS(A(\theta)). \tag{3}$$

Inserting (2) into (3) we obtain A_0 for the k-squared model with k-dependent rise time.

The spectral modification is illustrated in Fig. 4b. At frequencies higher than $2f_0$, the spectral amplitude is multiplied by $A_0/A(\theta)$. At transition frequencies between $1/2f_0$ and $2f_0$, the spectrum is modified by a cosine function to avoid a sharp step in the spectrum.

We apply this simple modification to the synthetics. The resulting PGAs and mean PGA map are shown in Fig. 5. As one can see, the PGA decay does not exhibit such strong azimuthal dependence as in the case of the k-squared model without correction (see Fig. 3). Moreover, all the PGAs now fall within the $\pm 2\sigma$ bounds around the empirical mean attenuation curve.

4 Discussion and conclusions

In this paper, we have compared two strong-motion modeling techniques with the empirical PGA attenuation relation, especially with the observed scatter. While the FSSD model

provides a variation in PGA by a factor of less than 10, the k-squared model provides a factor of about 100.

We attribute the large scatter in the k-squared model to the strong high-frequency directivity effect, not present in the FSSD model. We performed a number of tests with the k-squared model, varying input source parameters (e.g., v_r, L_0, shape of the slip velocity function) but we did not find that any of them reduced the scatter substantially. Note that the frequency-independent radiation pattern assumed in the k-squared model is not responsible for the very low PGA values in some directions (close to S-wave minima) because the same radiation pattern is present in the composite method as well. Moreover, we have tried to perform the computations with the k-squared model considering isotropic S-wave radiation with no significant change in the PGA scatter.

Many PGA attenuation relations provide an uncertainty by a factor of about 2 (Si and Midorikawa, 1999, Ambraseys et al., 2005, etc.). Thus, assuming $\pm 2\sigma$ criteria, the maximum total variation corresponds to a factor of about 16. Hence, the large scatter provided by the k-squared model in simple a 1D layered medium seems to overestimate the observed scatter.

One can understand the uncertainty in attenuation relations as an indirect empirical constraint on the physical parameters of the source model. However, we have found no parameter of the k-squared model which could significantly decrease the large synthetic scatter (except for putting the nucleation point position close to the center of the fault). Therefore, we apply a formal high-frequency spectral modification (suggested by Bernard and Herrero, 1994) to the k-squared method that eliminates the directivity due to rupture

propagation. The modification is formal and the physical reasons for small high-frequency directivity are unclear. A possible explanation is the incoherency at the source, as discussed above. However, the incoherency can also be caused by wave propagation in a 3D complex medium involving small-scale heterogeneities (e.g., O'Connell, 1999). The details of these phenomena are beyond the scope of this paper.

The 2004 Parkfield earthquake represents a unique opportunity to compare the very well recorded data of a predominantly unilateral earthquake with recent attenuation relations as it has provided an unprecedentedly detailed view of the PGA distribution at close fault distances. The majority of the PGA data fits between the $\pm 2\sigma$ bounds of the recent attenuation curve (Bakun et al., 2005) although the stations have not been classified according to their site conditions. Moreover, Shakal et al. (2006) report that there is no directivity dependence in the observed peak acceleration, which supports our results.

We believe that the standard deviation of the empirical attenuation relations represents robust information for calibration and possible rejection of strong-motion prediction methods. However, the data set has to be sufficiently large, including careful site classification and a large number of observations close (< 30 km) to the faults. The deployment of dense accelerometric networks in the last decade (in, e.g., Japan, USA, Taiwan) is very promising from this point of view. With this respect, our conclusion on the high-frequency directivity can be revised after more constrained (especially at fault distances smaller than 15km) attenuation relations are available. Note that the comparison between the synthetic and observed scatter cannot be used for technique validations until one takes into account all possible phenomena that boost the scatter (e.g., 3D structural effects, site effects, etc.).

Acknowledgments

The authors thank to Jiri Zahradnik, Johana Brokesova, Martin Mai, Antonio Emolo, Massimo Cocco, Giovanna Cultrera and an anonymous reviewer for their comments that helped to improve the manuscript. The work was supported by Marie Curie training network SPICE in the 6th Framework Program of the European Commission (MRTN-CT-2003-504267), Grant Agency of Charles University (279/2006/B-GEO/MFF) and by Italian National Institute of Geophysics and Volcanology and of the Italian Civil Defence Department.

References

Ambraseys N., Douglas J., Sarma S., Smit P., 2005. Equations for the Estimation of Strong Ground Motions from Shallow Crustal Earthquakes Using Data from Europe and the Middle East: Horizontal Peak Ground Acceleration and Spectral Acceleration. *Bulletin of Earthquake Engineering*, **3**, 1–53.

Bernard P. and Herrero A., 1994. Slip heterogeneity, body-wave spectra, and directivity of earthquake ruptures. *Annali di Geofisica*, Vol. **XXXVII**, 1679-1690.

Bernard P., Herrero A. and Berge C., 1996. Modeling directivity of heterogeneous earthquake ruptures. *Bull. Seism. Soc. Am.*, **86**, 1149-1160.

Boatwright J. and Boore D. M., 1982. Analysis of the ground accelerations radiated by the 1980 livermore valley earthquakes for directivity and dynamic source characteristics. *Bull.*

Seism. Soc. Am., **72**, 1843–1865.

Bouchon M., 1981. A simple method to calculate Green's functions for elastic layered media. *Bull. Seism. Soc. Am.*, **71**, 959–971.

Brune J., 1970. Tectonic stress and the spectra of seismic shear waves from earthquakes. *J. Geophys. Res.*, **75**, 4997-5009. (correction, *J. Geophys. Res.*, **76**, 5002, 1971).

Burjanek J., 2002. *A composite source model with fractal subevent size distribution.* Master Thesis, Charles University, Prague (Online at http://geo.mff.cuni.cz/∼burjanek/dipl.pdf).

Frankel A., 1991. High-frequency spectral fall-off of earthquakes, fractal dimension of complex rupture, b value, and the scaling strength on faults. *J. Geophys. Res.*, **96**, 6291–6302.

Gallovic F. and Brokesova J., 2004a. On strong ground motion synthesis with k^{-2} slip distributions. *J. Seismology*, **8**, 211–224.

Gallovic F. and Brokesova J., 2004b. The k^{-2} rupture model parametric study: example of the 1999 Athens earthquake. *Studia geoph. et geod.* **48**, 589–613.

Hartzell S., Harmsen S., Frankel A. and Larsen S., 1999. Calculation of broadband time histories of ground motion: comparison of methods and validation using strong-ground motion from the 1994 Northridge earthquake. *Bull. Seism. Soc. Am.*, **89**, 1484–1504.

Haskell N. A., 1964. Total energy and energy spectra density of elastic waves from propagating faults. *Bull. Seism. Soc. Am.*, **54**, 1811–1841.

Joyner W., 1991. Directivity for non-uniform ruptures. *Bull. Seism. Soc. Am.*, **81**, 1391-1395.

Margaris B. N. and Boore D. M., 1998. Determination of $\Delta\sigma$ and κ_0 from response spectra of large earthquakes in Greece, *Bull. Seism. Soc. Am.* **88**, 170-182.

McGuire, J. J., Zhao, L., Jordan, T. H. Predominance of Unilateral Rupture for a Global Catalog of Large Earthquakes, *Bull. Seism. Soc. Am.* **92**, 3309–3317.

NEHRP, 1994. *Recommended provisions for seismic regulations for new buildings and other structures, Part 1: Provisions*. FEMA 222A Building Seismic Safety Council, Washington D.C., 290 pp.

O'Connell D. R. H., 1999. Replication of apparent nonlinear seismic response with linear wave propagation models. *Science*, **283**, 2045-2050.

Plicka V. and Zahradnik J., 2002. Inversion of rupture nucleation from regional records by EGF method for unequal focal mechanisms of the mainshock and aftershock: the Athens 1999 earthquake. *Tectonophysics*, **359**, 81-95.

Si H. and Midorikawa S., 1999. New attenuation relationships for peak ground acceleration and velocity considering effects of fault type and site condition. *J. Struct. Constr. Eng., AIJ*, **523**, 63–70.

Skarlatoudis A. A., Papazachos C. B., Margaris B. N., Theodulidis N., Papaioannou Ch., Kalogeras I., Scordilis E. M. and Karakostas V., 2003. Empirical peak ground-motion predictive relations for shallow earthquakes in Greece. *Bull. Seism. Soc. Am.*, **93**, 2591-2603.

Somerville P. G., Smith N. F., Graves R. W. and Abrahamson N. A., 1997. Modification of Empirical Strong Ground-motion Attenuation Relations to Include the Amplitude and

Duration Effects of Rupture Directivity. *Seism. Res. Lett.*, **68**, 199-222.

Somerville P., Irikura K., Graves R., Sawada S., Wald D., Abrahamson N., Iwasaki Y., Kagawa T., Smith N. and Kowada A., 1999. Characterizing crustal earthquake slip models for the prediction of strong ground motion. *Seism. Res. Lett.*, **70**, 59–80.

Tselentis G. A. and Zahradnik J., 2000. The Athens Earthquake of 7 September 1999. *Bull. Seism. Soc. Am.*, **90**, 1143–1160.

Zahradnik J., 2002. *Focal mechanism of the Athens 1999 earthquake by ASPO method.* Res. Report, Dept. of Geophysics, Faculty of Math. and Phys., Charles University, Prague (Online at http://seis30.karlov.mff.cuni.cz/papers/aspo/aspo.html).

Figure captions

Figure 1: An example of one random realization of the slip distribution employed in the k-squared method. The star denotes the nucleation point.

Figure 2: A comparison of full wavefield and direct S-wave accelerograms (k-squared model) for one selected station marked in Fig. 3B.

Figure 3: A) Maps of PGA (in m/s^2) averaged over 10 realizations of stochastic source models. Receivers are shown as triangles. The rectangles represent the fault and asperity surface projections. The stars in the middle of the maps correspond to the epicenter. The gray dashed lines represent fault traces on the surface. The highlighted receiver in the right panel relates to Fig. 2. B) All simulated PGAs (symbols) plotted versus epicentral distance obtained for the first 5 realizations. The PGAs corresponding to different realizations are plotted with different symbols and are slightly shifted in the x-direction for better viewing in order to highlight the scatter of each realization. The strips of symbols appear due to the circular layout of the stations. The gray strokes denote PGA means at given epicentral distances of all 10 realizations. The mean empirical PGA attenuation curve and corresponding $\pm 2\sigma$ (Skarlatoudis et al., 2003) are depicted by dashed and solid lines, respectively.

Figure 4: a) Theoretical acceleration source spectra of the k-squared model with k-dependent rise time for a line fault in the Fraunhofer approximation for various angles θ from the direction of rupture propagation (after Gallovic and Brokesova, 2004a). b) Same as a), but with formal spectral modification applied in this paper. Note that this figure is only schematic and we do not expect such sharp changes in the observed spectra. The transition could be smoother and/or would be masked by the oscillatory character of the Fourier spectra.

Figure 5: Same as the right-hand plots in Fig. 3 (k-squared model) after incorporating the formal spectral modification illustrated in Fig. 4.

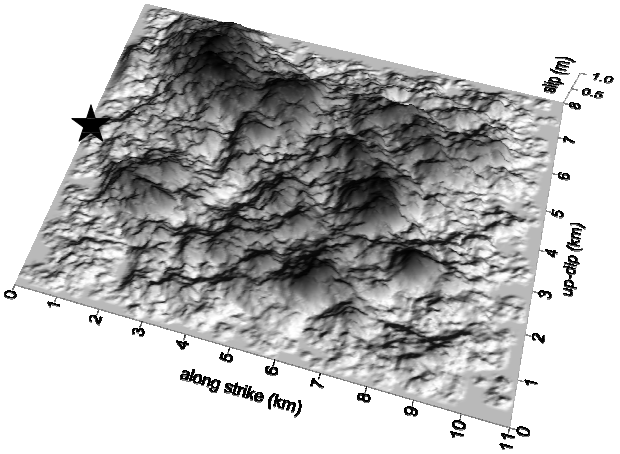
slip (m)
1.0
0.5
0
1
2
3
4
5
6
7
8
up-dip (km)
0
1
2
3
4
5
6
7
8
9
10
11
along strike (km)

Fig. 1

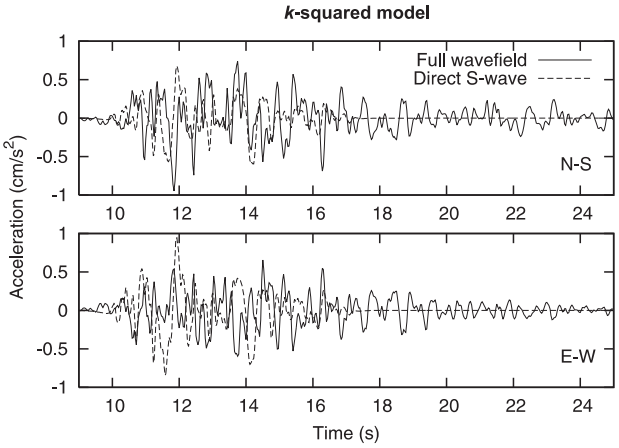
k-squared model
Full wavefield
Direct S-wave
N-S
E-W
Acceleration (cm/s^2)
Time (s)
1
0.5
0
-0.5
-1
10
12
14
16
18
20
22
24

Fig. 2

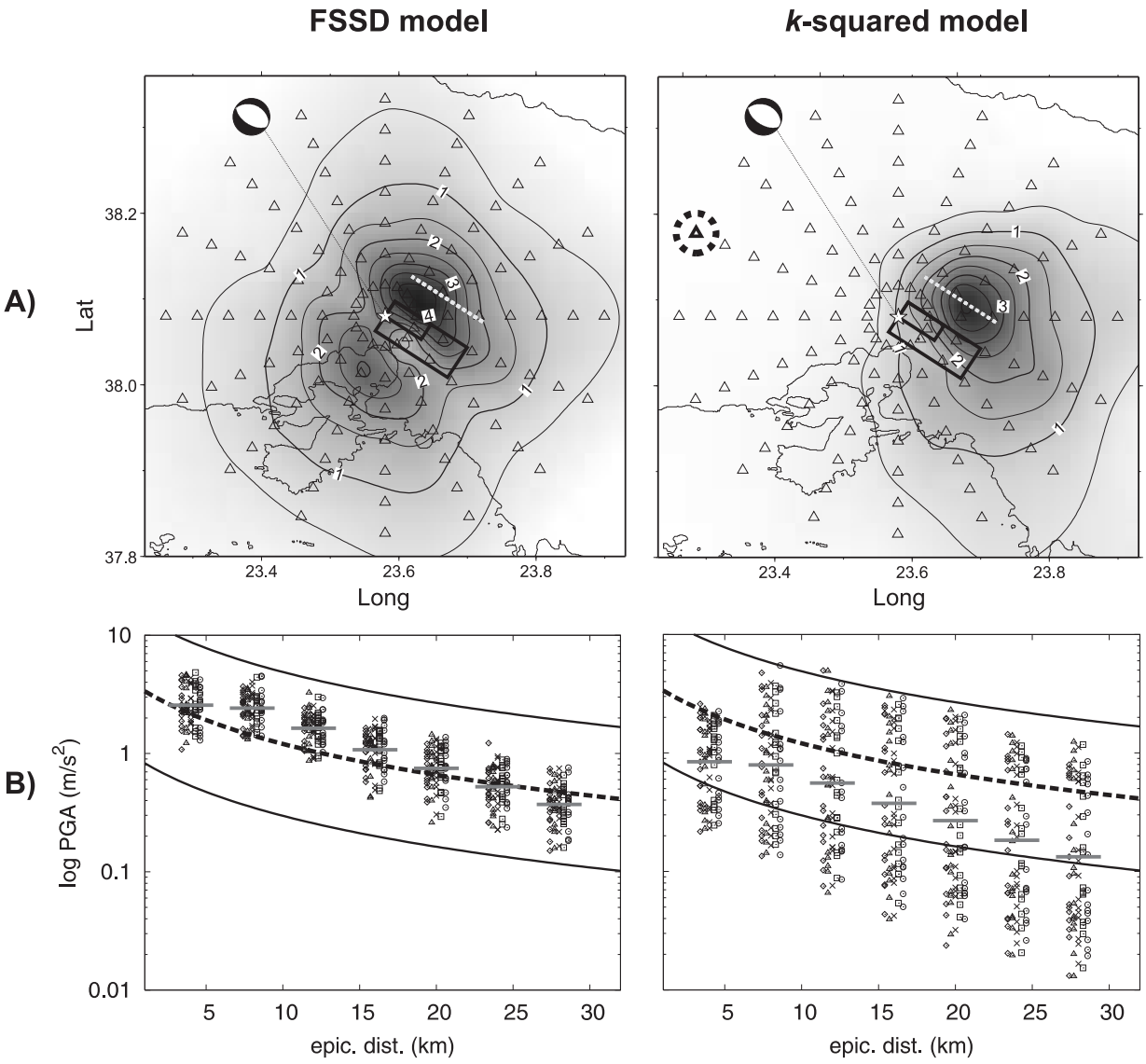
FSSD model
k-squared model
A)
B)
Lat
Long
38.2
38.0
37.8
23.4
23.6
23.8
log PGA (m/s^2)
epic. dist. (km)
10
1
0.1
0.01
5
10
15
20
25
30

Fig. 3

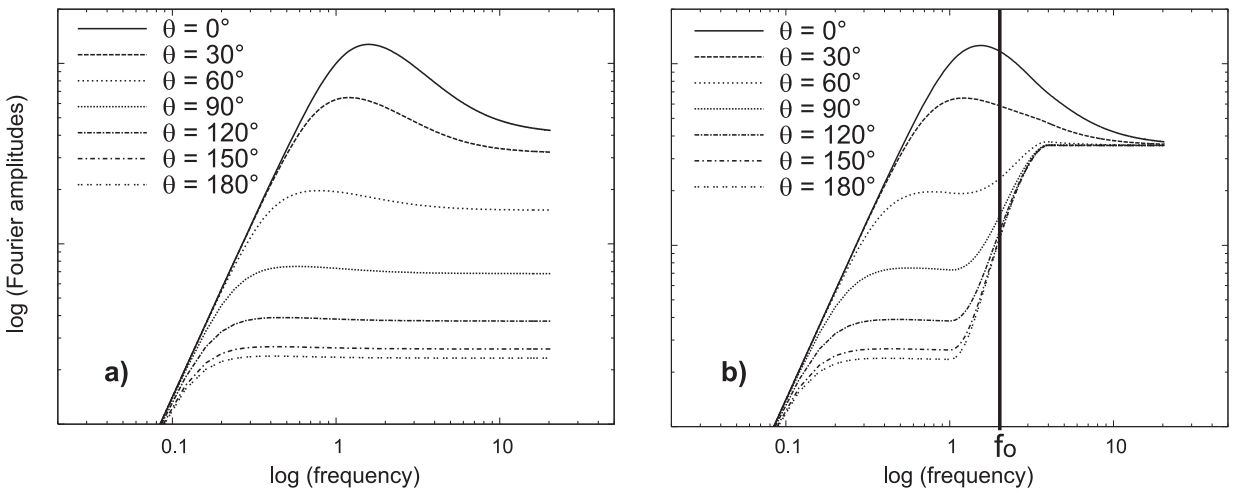
θ = 0°
θ = 30°
θ = 60°
θ = 90°
θ = 120°
θ = 150°
θ = 180°
log (Fourier amplitudes)
a)
0.1
1
10
log (frequency)
b)
fo

Fig. 4

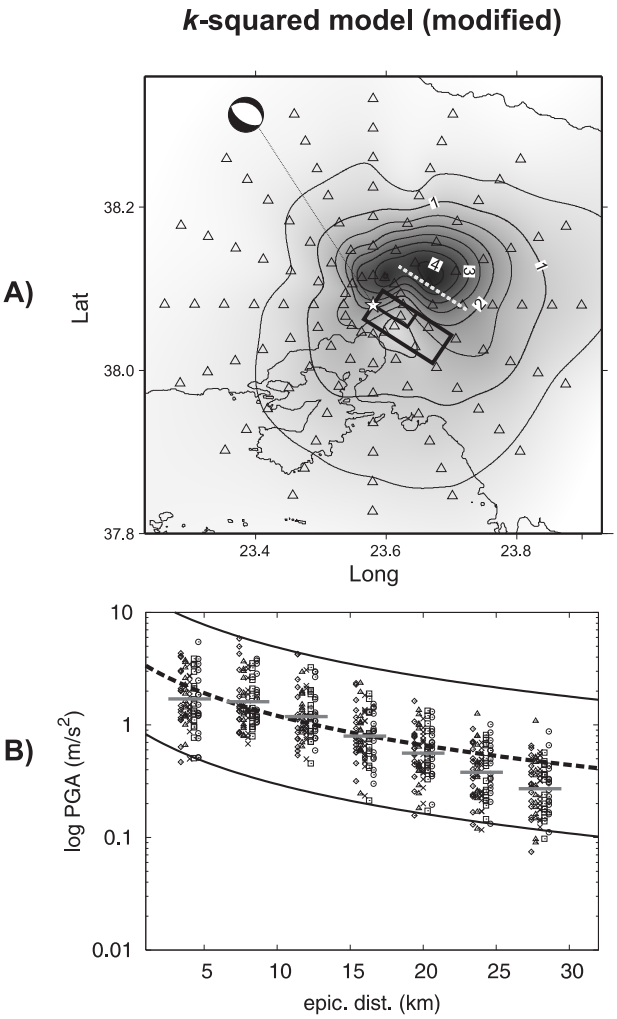
k-squared model (modified)
A)
Lat
38.2
38.0
37.8
23.4
23.6
23.8
Long
B)
log PGA (m/s2)
10
1
0.1
0.01
5
10
15
20
25
30
epic. dist. (km)

Fig. 5